Image-space surface-related multiple prediction

Brad Artman[1]**, Gabriel Alvarez**[1]**, and Ken Matson**[2]

brad@geo.stanford.edu

[1]*Stanford Exploration Project, Mitchell Bldg., Department of Geophysics,*

Stanford University, Stanford, CA 94305-2215

[2]*BP , 200 Westlake Park Blvd., Houston, Texas, 77079*

GEO-2006-0199-R1

Submitted: September 28, 2006

RESPONSE

New text is *italicized and red*. If more than a few lines, lots of new text is framed.

Removed text is ~~blue and struck-out.~~ File `artman.pdf` contains only the fresh text. File `rev.artman.pdf` shows edits.

As it was my intention to tend toward brevity and focus only on prediction, I did not want to include the subjects of performance and subtraction in this submission. However, the bulk of the reviews requested subtraction results. Thus, in addition to the suggestions directed specifically at presentation and clarity, I have elicited the help of a new co-author to address issues surrounding the removal of the multiples after prediction. This adds significantly to the length of the paper and contributes substantially to the "major" in major revisions (i.e. lots of new (red) text).

I hope you all like my sexy new figures. The old Figure 1 was a waste of space, the new Figure 1 is a very nice sketch cartooning the development of the predictionduring the course of extrapolation.

Some of your comments have been incorporated almost verbatim in the text when your phrasing was particularly succinct. Those who made the effort to provide thorough reviews should get a publishing credit as far as I'm concerned. Thank you Mssrs. W, V, and S.

The abstract was universally dismissed, and so is re-written completely without

inclusion of its previous form.

A substantial amount of red (new) ink is associated with remarks concerning amplitudes. I have also added a simple synthetic and real data example for your viewing pleasure.

Deconvolution imaging conditions did not perform as well as had I hoped, and seemed distracting. Therefore, I've removed all mention of the idea. (If anyone's interested, the deconvolved multiple prediction always has very faint primaries in it. Can't figure out why.)

The applicability of this idea to DSR migrations is now referenced as I found out last week there are other authors moving such a paper through this same review process currently.

Extrapolation equations are re-written without reference to Fourier domain variables, since implementation is mixed-domain, the new form is more parallel with the various imaging conditions (and it really doesn't matter anyway). While, I believe, this somewhat obscures the commutability claim, I hope that this addresses the worry that the method could be construed as only applicable to laterally invariant media.

Abstract

A very important aspect of removing multiples from seismic data is accurate prediction of their kinematics. We recast the multiple prediction problem as an operation in the image space parallel to the conventional surface-related multiple prediction methodology. Though cast in the image domain, the technique shares the data-driven strengths of data-domain surface-related multiple elimination (SRME) by being independent of the Earth (velocity) model, or the accuracy of kinematic descriptions of the multiples or primaries as is important in methods relying on Radon transforms. The cost of the prediction is approximately the same as data-space methods, though it can be computed during the course of migration. Its additive cost is not significant to that incurred by shot-profile migration.

Image-space multiple predictions are manufactured by auto-convolving the traces in each shot-gather at every depth level during the course of a shot-profile migration. The prediction in the image domain is equivalent to that produced by migrating the data-space convolutional prediction. Adaptive subtraction of the prediction from the image is required. Subtraction in the image domain however provides the advantages of focused energy in a smaller domain since extrapolation removes some of the imperfections of the input data.

INTRODUCTION

It is well known that removing multiples from seismic data is an imperative to producing interpretable images of the subsurface. Multiple attenuation has a rich history in the geophysical literature ranging from methods that try to predict and remove the multiples from the seismic data to methods that use a differential characteristic between primaries and multiples as a discriminator and the basis for separating the two types of events (Weglein, 1999).

Prediction of the kinematics of multiple reflections by convolution of recorded data was first suggested by Anstey and Newman (1966). Due to amplitude and bandwidth inconsistencies associated

with convolution, direct subtraction of multiples thus predicted was not possible. Tsai (1985) suggests modeling the waveform of the multiples to subtract events at times calculated by convolution from the data. The surface-related multiple elimination (SRME) method (Verschuur et al., 1992; Berkhout and Verschuur, 1997) convolves traces within shot-gathers to predict multiples (surface-related multiple prediction, SRMP) followed by an iterative subtraction scheme to eliminate them from the data. Alternatively, after predicting multiples, via convolution or filter-based methods, Guitton (2005) uses a pattern-based subtraction technique that resembles the match filter application described in Biersteker (2001).

While the above references all operate in the data domain, authors have also suggested removing multiples in the image space, after migration (Sava and Guitton, 2003, 2005; Alvarez et al., 2004). These authors capitalize on kinematic differentiation of the primaries and multiples and separate the two via a Radon transform tailored to residual moveout or the analytic expression of over-migrated multiples, respectively. There are several motivators for attacking multiples in the image space. First, the image space is usually much smaller than the data space. Second, given a reasonably accurate velocity model, the kinematics of the image domain are simplified. Appropriately migrated primary events have little to no residual moveout, and multiples, migrated with velocities that are too fast, have predictable moveout in both angle- and offset-domain common-image gathers. Alternatively, one could migrate the data and a data-domain multiple prediction separately and subtract the two image volumes. This is probably a prohibitively expensive strategy. However, null-traces in the data are filled during extrapolation steps as energy propagates laterally during down-ward continuation. This may help multiple predictions in the image space to be more continuous and accurate in 3D.

We extend the SRMP approach to the image domain through the commutability of wavefield extrapolation and convolution to produce a multiple prediction in the image domain without needing to migrate two data volumes. Our approach is directly analogous to SRMP, though the prediction

is calculated during the course of a shot-profile migration. The added cost of image-space surface-related multiple prediction (IS-SRMP) is only a second imaging condition. Because extrapolation dominates the cost of migration, IS-SRMP does not significantly increase its cost. Generating a multiple model in the image domain during DSR migrations was also discussed in Malcolm et al. (2006). Because the upcoming and downgoing energy are not explicitly separate, as in shot-profile algorithms, the authors require extra work that is not necessary for this method. That extra work effectively doubles the the cost of the (DSR) migration. In contrast to our method, it implicitly acts in a layer-stripping methodology that is also capable of predicting intrabed multiples.

The multiple prediction produced in the image space with this technique is mathematically equivalent to migrating the multiple prediction produced by SRMP convolutions. The predicted multiples are then removed from the data via adaptive subtraction or pattern-matching techniques. The need for adaptive subtraction is two-fold. First, convolution squares the wavelet in the data which halves the bandwidth, squares the amplitude, and destroys the polarity of the output. Therefore, even if a true-amplitude migration algorithm is available, the multiple prediction will not share the amplitude characteristics of the multiples in the migrated image. Second, adaptive subtraction can account for imperfections including kinematic errors and the presence of primaries or higher-order multiples in the prediction.

As wave-equation migration becomes more of a commodity, iterative migration as part of estimating the Earth's velocity has become more common. The presence of multiples in the data makes velocity analysis more difficult since events are present at the same time or depth with conflicting velocity properties. For this reason, there will always be reason to remove multiples in the data domain. However, if a shot-profile migration strategy is planned, it will be shown that simultaneously producing a multiple prediction adds no significant cost, and does not require the presence of multiples in the data being migrated. Therefore, the prediction can be generated even after perfect elimination as

a comparative volume for interpreters to use as an example of events that are not geologic.

We develop the image-space surface-related multiple prediction (IS-SRMP) technique by combining the SRMP approach with a wave-equation shot-profile depth migration algorithm. Guitton (2005) shows that pattern-based and adaptive subtraction of multiple models work better when higher dimensionalities can be exploited by the subtraction algorithm. The various imaging conditions we present can all produce the image as a function of subsurface offset (and from there reflection angle) to facilitate better subtraction. A simple flat-layer synthetic and the Sigsbee2B synthetic data set are used to show the efficacy of the prediction and its subtraction from the migrated image. Multiple prediction and subtraction is also presented from a Gulf of Mexico data set acquired by Western-Geco in the Mississippi Canyon lease area.

IMAGE-SPACE SRMP

The image space is the output of migration, which we produce with a shot-profile depth migration algorithm. Shot-profile wave-equation depth migration (Claerbout, 1971) is the cascade of two component operations: extrapolation and imaging. Extrapolation is carried out with an anticausal wave-equation operator applied to the up-going wavefield, U, and a causal operator applied to the down-going wavefield, D. U is a shot record with traces placed along a wavefield axis $\mathbf{x}$. D is a zero valued wavefield, also defined along the axis $\mathbf{x}$, where a source function is placed at the location of the shot being migrated, $\mathbf{x}_s$. The wavefields are recursively extrapolated to all depths z using one-way mixed-domain solutions to the wave-equation

$$U_{z+1}(\mathbf{x};\mathbf{x}_s,t) \quad = \quad E^+(\mathbf{x},t)U_z(\mathbf{x};\mathbf{x}_s,t) \tag{1}$$

and

$$D_{z+1}(\mathbf{x};\mathbf{x}_s,t) \quad = \quad E^-(\mathbf{x},t)D_z(\mathbf{x};\mathbf{x}_s,t)\,. \tag{2}$$

In this work, the form of the extrapolator E used to propagate the wavefields is the split-step Fourier plus interpolation (SSF-PI) (Kessinger, 1992) with multiple reference velocities, though the degree of complexity of the operator does not change the discussion herein. The importance of these equations is that the operator that extrapolates a wavefield from one depth level to the next is commutable with convolution. Using the simple, though less accurate, bulk phase-shift operator of the form $e^{i\omega k_z}$ for E, makes this commutativity more obvious.

The correlation based multi-offset imaging condition for shot-profile migration is (Rickett and Sava, 2002)

$$i_z(\mathbf{x},\mathbf{h}) = \sum_{\mathbf{x}_s}\sum_{\omega} U_z(\mathbf{x}+\mathbf{h};\mathbf{x}_s,\omega) D_z^*(\mathbf{x}-\mathbf{h};\mathbf{x}_s,\omega) \tag{3}$$

where the $*$ represents conjugation, and $\mathbf{h}$ is subsurface offset. Extraction of the zero lag of the correlations, by summation over ω, combines the energy in the two wavefields that is collocated at each depth level. Overlapping acquisition patches from the individual shots are stacked by the sum over $\mathbf{x}_s$.

Acknowledging the approximation of convolving raw data traces rather than data with only primaries, the prediction of multiples in the data domain (SRMP) can be written in the Fourier domain (Berkhout and Verschuur, equation 13f, 1997)

$$M(\mathbf{x}_g;\mathbf{x}_s,\omega) = \sum_{\mathbf{x}_a} R(\mathbf{x}_g;\mathbf{x}_a,\omega) R(\mathbf{x}_a;\mathbf{x}_s,\omega)\,, \tag{4}$$

where R is the data-space volume of shot-gathers defined at geophone and source locations on the acquisition surface. Equation 4 is a trace-by-trace operation to produce the multiple prediction with any geophone-source, $(\mathbf{x}_g,\mathbf{x}_s)$, combination by convolving each trace of every shot gather with all the others followed by summing over the convolution index $\mathbf{x}_a$. Note however, the similarity of the SRMP equation to the imaging condition of shot-profile migration, equation 3.

Wave-equation extrapolation is performed on wavefields where data and source-functions are

used as initial conditions to propagate energy into the subsurface. To begin, traces at locations $\mathbf{x}_g$ are inserted into a zero-valued wavefield defined along the axis $\mathbf{x}$. Although data-space SRMP is a trace-by-trace operation, equation 4 can be redefined in terms of the wavefield $U(\mathbf{x},\mathbf{x}_s)$. With null-traces at locations $\mathbf{x}$ where no data were collected, a multiple prediction can also be written

$$M_{z=0}(\mathbf{x};\mathbf{x}_s,\omega) = \sum_{\mathbf{x}_a} U_{z=0}(\mathbf{x};\mathbf{x}_a,\omega)U_{z=0}(\mathbf{x}_a;\mathbf{x}_s,\omega)\,, \tag{5}$$

where we have added the specification that the operation is being performed at the recording surface $z = 0$.

Using the principle of reciprocity between the receiver and source locations (first and second arguments of the wavefields respectively), the multiple prediction becomes

$$M_{z=0}(\mathbf{x};\mathbf{x}_s,\omega) = \sum_{\mathbf{x}_a} U_{z=0}(\mathbf{x};\mathbf{x}_a,\omega)U_{z=0}(\mathbf{x}_s;\mathbf{x}_a,\omega)\,. \tag{6}$$

Here, the subscript s on the RHS represents any different receiver location (since it is the first argument of the wavefield), and the dummy index $\mathbf{x}_a$ is recognized as a summation over source location. Therefore, using arbitrary index subscripts c,d and restoring the significance of source location to subscript s

$$M_{z=0}(\mathbf{x}_c;\mathbf{x}_d,\omega) = \sum_{\mathbf{x}_s} U_{z=0}(\mathbf{x}_c;\mathbf{x}_s,\omega)U_{z=0}(\mathbf{x}_d;\mathbf{x}_s,\omega)\,. \tag{7}$$

Finally, we define the dummy indices c,d in terms of physically significant variables location and half-offset, $\mathbf{x}_c = \mathbf{x}+\mathbf{h}$ and $\mathbf{x}_d = \mathbf{x}-\mathbf{h}$, such that

$$M_{z=0}(\mathbf{x},\mathbf{h},\omega) = \sum_{\mathbf{x}_s} U_{z=0}(\mathbf{x}+\mathbf{h};\mathbf{x}_s,\omega)U_{z=0}(\mathbf{x}-\mathbf{h};\mathbf{x}_s,\omega)\,. \tag{8}$$

Thus reconfigured, equation 8 is now of parallel construction to the shot-profile imaging condition, equation 3, lacking only the summation over frequency.

Extrapolation by $E(\mathbf{x},\mathbf{t})$, in equation 1, simply redatums the shot-gather U. Image-space SRMP (IS-SRMP) is the application of a second imaging condition evaluated at each subsurface depth level

during the migration that images only multiples. It is the chain of multiple prediction (convolution) and zero-time extraction (summation over frequency). The image-space multiple prediction, as a function of sub-surface offset, is therefore

$$m_z(\mathbf{x},\mathbf{h}) = \sum_{\mathbf{x}_s}\sum_{\omega} U_z(\mathbf{x}+\mathbf{h};\mathbf{x}_s,\omega)U_z(\mathbf{x}-\mathbf{h};\mathbf{x}_s,\omega)\,. \tag{9}$$

There are two important ramifications associated with the equation for predicting multiples with the imaging condition above. The first is that this operation is intrinsically a shot-domain manipulation of the data. After sorting to midpoint-offset coordinates, the source and receiver coordinates are mixed in such a way as to make IS-SRMP more difficult for survey-sinking style migration algorithms (Malcolm et al., 2006). Second,because reciprocity was invoked to derive equation 9, off-end (marine) acquisition geometries will need to have split-spread gathers manufactured via reciprocity. The split-spread gathers will include the ray-paths from multiples that emerge in front of the receiver spread (boat) which need to be included in the shot-gathers to predict all possible multiple events.

Further understanding of the IS-SRMP imaging condition for those familiar with shot-profile migration algorithms can be elicited by defining the down-going wavefield in equation 2 as $D \equiv U$. Therefore, equations 1 - 3 become

$$U_{z+1}(\mathbf{x};\mathbf{x}_s,t) \quad = \quad E^{-}(\mathbf{x},t)U_z(\mathbf{x};\mathbf{x}_s,t) \tag{10}$$

and

$$\hat{U}_{z+1}(\mathbf{x};\mathbf{x}_s,t) \quad = \quad E^{+}(\mathbf{x},t)\hat{U}_z(\mathbf{x};\mathbf{x}_s,t) \tag{11}$$

with the the imaging condition

$$i_z(\mathbf{x},\mathbf{h}) = \sum_{\mathbf{x}_s}\sum_{\omega} U_z(\mathbf{x}+\mathbf{h};\mathbf{x}_s,\omega)\hat{U}^{*}_z(\mathbf{x}-\mathbf{h};\mathbf{x}_s,\omega)\,, \tag{12}$$

where $\hat{}$ denotes that after extrapolation in different directions, the wavefields are no longer identical. Because the conjugation of D in the imaging condition of equation 3 can be commuted with the

causality of the extrapolation operator, it is not necessary to extrapolate U in two different directions. Instead, the second extrapolation above can be ignored and the imaging condition becomes convolutional rather than correlational. In this case, equation 12 is exactly the multiple prediction, equation 9. Cast in this manner, the migration shows similarity with reverse-time migration (Baysal et al., 1983) and using multiples to migrate primaries (Shan and Guitton, 2004). The difference is that the data used as source function is not first time-reversed. IS-SRMP uses the data as both areal source functions and data to image multiples. Conversely, time-reversing the data will use the primaries as areal source functions (delayed from time zero) to image the subsurface with the multiple reflections. Using both an impulsive source function at $\mathbf{x}_s$ and time-reversed primaries as a source function would image Earth structure with the primaries and the multiples, but still include the multiples in the image.

Analytic example

In 1D, let a trace be represented in the Fourier domain by the expression

$$R(\omega) = \mathrm{e}^{-i\phi_w} + \mathrm{e}^{-i\phi_e} - \mathrm{e}^{-i2\phi_w} - 2\mathrm{e}^{-i(\phi_w+\phi_e)} - \mathrm{e}^{-i2\phi_e} = P + M_1. \tag{13}$$

The trace has primary reflections, P, at phase delays, ϕ, representing a water-bottom and a subsurface event. Also included are first order multiples, M_1, which are the water-bottom multiple at $2\phi_w$, two peg-leg multiples at $\phi_w + \phi_e$, and the event multiple at $2\phi_e$. SRMP dictates the autoconvolution of P to derive M_1, which is clearly true. Including the events M_1 in the autoconvolution will predict the higher-order multiples as well.

Extrapolating trace R to a deeper depth applies a common phase shift, say $\mathrm{e}^{-i\phi_z}$, to all terms in equation 13. The trace then becomes

$$R_z(\omega) = e^{-i\phi_z}(\mathrm{e}^{-i\phi_w} + \mathrm{e}^{-i\phi_e} + \mathrm{e}^{-i2\phi_w} + 2\mathrm{e}^{-i(\phi_w+\phi_e)} + \mathrm{e}^{-i2\phi_e}) = e^{-i\phi_z} P + e^{-i\phi_z} M_1. \tag{14}$$

This equation shows that the extrapolation of data without multiple subtraction produces the superposition of the redatumed primaries and the redatumed multiples. The extraction of the zero-time lag in the imaging condition of migration states that energy in the wavefield should be mapped into the image domain only when the extrapolation phasor ϕ_z, is equal to the time delay of the event in the data. Thus the water bottom primary is imaged when $\phi_z = \phi_w$, the water-bottom multiple is imaged when $\phi_z = 2\phi_w$, etc. Whether the data R is first separated into its constituent parts, P and M_i, or not, it can be seen where in the image domain the various events in the above example will be placed. However, by first squaring the trace, implementing data-space SRMP, the water-bottom primary is mapped into the image domain when $\phi_z = 2\phi_w$. This is the same phasor that maps the recorded water-bottom multiple into the image domain when migrating data contaminated with multiples.

Figure 1 is a cartoon depicting the generation of a 1D image-space surface-related multiple prediction without first convolving the gathers. The scenario drawn is for the simple case of a water-bottom reflector and its multiple. The trace U denotes a zero-offset recording from a shot gather, and D is the modeled source function used for shot-profile migration. The trace I represents the result of the conventional imaging condition, while M is the multiple prediction in the image space generated by auto-convolution. The superscript $*$ denotes conjugation. Both imaging conditions only extract energy at $t = 0$.

Figure 1 about here

The first panel, $z = 0$, shows the initial conditions of U and D and the fact that both $I|_{t=0}$ and $M|_{t=0}$ are devoid of events. Since correlation subtracts the time of energy in the source trace D, currently zero, from the receiver trace, U, the image trace $I = U$. The time for events on trace UU are doubled from the initial condition, which results in the multiple on trace U mapping below the time interval shown the cartoon.

The second panel depicts the situation when the wavefields have been extrapolated to the depth of the water column. Now energy in D and U is collocated and the primary is imaged during correlation, UD^*. The multiple prediction is still zero valued. The last panel depicts the wavefields and imaging results after the wavefields have been propagated to twice the depth of the water column. Now the source energy is collocated with the multiple, and the correlation results in a negative polarity event. Simultaneously, the primary is now at $t = 0$ which maps energy into the IS-SRMP volume, M. However, even though the kinematics of the multiple in UU are correct, the event has the wrong polarity. Also notice that the multiple is now at the original time of the primary, which sets up prediction of second-order multiples from the convolution of the first-order multiples. Importantly, this also shows that U consisting of only primaries will correctly predict the location of multiples even if no multiples exist in the data. Also, even if the velocity used to calculate the extrapolation phasors is incorrect, both I and M will share the same error.

Simple synthetic

The left panel of Figure 2 is a synthetic shot gather with two reflections and three multiples. The velocity to the first flat layer at depth $z = 400$ m is 1500 m/s. The velocity is 2500 m/s to the second flat layer at depth $z = 1200$ m. The kinematics were computed analytically and convolved with a wavelet. The white events are primaries, and the multiples have opposite polarity. The three multiple events are the simple multiples to both events, and the asymmetric peg-leg. The intrabed multiples between the two layers were not included since they are not predicted by SRMP. Receiver and source spacing was 20 m. The right panel is a subsurface-offset common-image gather produced by shot-profile migration of 350 shot-gathers identical to the data shown. The velocity model was two layers: 1500 m/s over 2500 m/s. Because the layers are flat, every location $\mathbf{x}$, away from the edges, is the same. Only $1/6^{th}$ of the subsurface offsets are required to capture the moveout of events after

migration.

Figure 2 about here

The two panels in Figure 3 are offset-domain common-image gathers produced by migrating only the primaries in the data above. The first panel shows energy tightly focused at zero offset for the two reflectors. The second panel is the multiple prediction. Three clear events are imaged with concave-up moveout. The middle event is the peg-leg multiple and the others are the simple multiples to the two reflectors. At zero-offset, the events are analytically calculated to arrive at depths $z = 1066, 1866$ and 2666 m, respectively.

Figure 3 about here

The two panels in Figure 4 are offset-domain common-image gathers produced by migrating all the events in Figure 2. Auto-convolution predicts multiples from primaries. Convolution of primaries with the multiples produces second-order multiples. Auto-convolution of multiples predicts third-order multiples. The left panel now has the two focused primary events and the three multiples predicted by IS-SRMP in Figure 3. These multiples are again predicted in the IS-SRMP gather on the right of this figure. However, higher order multiples are now included as well. The broad event at $z = 1733$ m is the multiple that makes three trips through the water column. The faint event at $z = 2400$ m is the double water-column multiple. The last new event is at $z = 2533$ m. This multiple has two trips in the water column and one trip from the surface to the second reflector.

Figure 4 about here

Sigsbee2B synthetic

The Sigsbee2B data-set was designed to model strong surface-related multiples from an offshore acquisition. Two datasets were generated with a 2D finite difference algorithm: One with the perfectly reflecting free surface, and one without[1]. Therefore, the direct subtraction of the two data volumes yields a nearly perfect multiple model without the need for SRMP. There are slight differences in the source and receiver ghost effects between the two data sets, so their subtraction retains faint residuals of primary energy. Though the data were modeled with an off-end acquisition strategy, split-spread gathers were computed via reciprocity for all of the examples below. All of the images herein were produced with four reference velocities in a SSF-PI shot-profile migration code.

Figure 5 shows zero subsurface-offset images of the Sigsbee2B data set. The top panel, generated with the conventional imaging condition, contains primaries and multiples. The bottom panel has multiples and some migration artifacts. The worst artifacts in the prediction are above the first multiple, especially near steep salt flanks. This noise can be easily muted before subtraction. The IS-SRMP image was produced using the data with primaries only. The data was modeled such that the details of the bottom left corner have simple kinematic differences between primaries and multiples: Events dipping up-right are multiples, and those dipping down-right are primaries.

Figure 5 about here

Figure 6 shows the bottom third of the image produced with the Sigsbee2B data sets. The top image used the data modeled without the reflecting free surface and contains only primaries. The second image migrated the data with the free-surface and contains multiples. The third panel is the image produced by migrating the difference between the two modeled data volumes (only multiples). The complex multiples in this deep section quickly overwhelm the primary events and could easily

[1] http://www.delphi.tudelft.nl/SMAART/S2Breadme.htm

be mistaken for primaries in some instances. Notice the faint primaries in the top left corner and the basement reflector due to the imperfect subtraction. The bottom panel is a zoomed in version of the multiple prediction in Figure 5. No residual primaries are present, but some edge effects are visible at $z = 6000$ m on the left side. The bottom two panels are effectively identical which demonstrates the commutability of SRMP convolutions and shot-profile migration.

Figure 6 about here

Gulf of Mexico data

The left panel of Figure 7 is a shot gather from a data set acquired in 1997 by Western-Geco in the Mississippi Canyon lease area of the Gulf of Mexico. Split-spread coverage was generated via reciprocity. The data set contains 1096 shots and recorded to 10 s. The source and receiver sampling was 27 m. The right panel is a angle gather from the same location. The raw data contains 367 traces, while the angle gather contains only 60 traces. Primaries are well flat, and multiples have characteristic concave-down shape. Before migration, the data were regularized, and bandpassed from 3-65 Hz. The data were migrated with the same SSF-PI shot-profile migration algorithm with four reference velocities. For zero-offset migration, the cost of the imaging condition, including the multiple prediction, was 1.4% of the cost of extrapolation. Calculating 60 subsurface offsets approximately equalizes the costs of extrapolation (with four reference velocities) and imaging (including multiple prediction and conventional image generation). This number of offsets is about $1/6^{th}$ of the traces in the split-spread gather, and more than sufficient to capture the unfocused multiple energy at all depths in the subsurface-offset gathers.

Figure 7 about here

Figure 8 shows the resulting migration and image-space multiple prediction. The multiples have the opposite polarity as expected. The quantity of multiple events in the prediction is overwhelming. Several events in the deep section of the image that have correspondence in the multiple prediction, look very much like primaries. The event that runs off the image at 2 km could very easily be misinterpreted as a primaries. Below the salt bottom and above the first water-bottom multiple, several intrabed multiples can be identified in the image that are not predicted in this context.

Figure 8 about here

SUBTRACTION

After predicting the kinematics of the multiples, they must be adaptively subtracted from the image due to the amplitude and bandwidth problems associated with convolving (squaring) the traces. Another potential problem with generating a multiple prediction by convolving data instead of only the primaries is the prediction of higher-order multiples, even if they were not recorded in the time interval of the original data. This was noted above in the IS-SRMP predictions with the flat-layer synthetic, Figure 4. The adaptive subtraction must be able to ignore events in the multiple prediction that are completely absent from the data. Also, the multiple prediction has more artifacts than the image. This is especially true at shallow depths before the first multiple. These artifacts must not be introduced to the estimate of the primaries when removing the multiples.

In this section we present subtraction results from the previous predictions using adaptive subtraction. Adaptive subtraction proceeds by inverting match filters connecting two similar objects, convolving the filter bank with its object, and subtracting this result from the second object. This can be a complicated and subtle art that we make no claims in performing at the optimum level. All subtraction results presented operated in two dimensions, and could likely be improved (Guitton, 2005)

by incorporating more dimensions in the process.

We pose the subtraction of the predicted multiples from the data as the following linear inversion problem:

$$\mathbf{Mf} \approx \mathbf{d} \tag{15}$$

$$\epsilon\mathbf{Af} \approx \mathbf{0}, \tag{16}$$

where $\mathbf{M}$ is the convolutional matrix of the multiples (a matrix whose columns contain shifted versions of a vector of the multiple prediction, $\mathbf{m}$), and $\mathbf{f}$ is a bank of non-stationary filters acting on patches (Claerbout and Fomel, 2002) of the data vector, $\mathbf{d}$, which contains primaries and multiples. The matrix $\mathbf{A}$ is a regularization operator (in this case a Laplacian) and ϵ is the standard factor to control the amount of regularization. The result of this linear inversion is a multiple model, $\mathbf{mf}$, that matches the amplitude and wavelet of the data.

Simple synthetic

Figure 9 details the steps in the subtraction process for a angle-domain common-image gather from the flat-layer synthetic. The first panel is the conventional image. The second panel is the IS-SRMP gather. The last panel is the matched version of the IS-SRMP gather, $\mathbf{mf}$, ready to subtract from the image gather. Some energy from the water-bottom primary has leaked into matched multiple prediction. Where the first multiple crosses the second primary, the filters have difficulty separating the two events. The higher-order multiples at the bottom of the initial prediction have been very effectively removed.

Figure 9 about here

Figure 10 contains final subtraction results. The first panel is the subtraction of the first and third panels in the previous figure, $\mathbf{d} - \mathbf{mf}$. This is a reasonable result, but suffers from some artifacts. The last panel is the original image gather, $\mathbf{d}$. The improved subtraction result in the center is produced with a second application of the the match-filter technique described in equation 15. For this application, the convolutional matrix $\mathbf{M}$ is made from the subtraction result (first panel), and the data vector $\mathbf{d}$ is once again the conventional image gather. The result shown is therefore the subtraction result matched to the input gather.

Figure 10 about here

Missing data, either source or receiver positions, results in incomplete multiple prediction for SRMP. However, extrapolation spreads energy across such gaps after a few propagation steps. This is commonly referred to as wave-front healing. Collecting near-offset traces is always difficult in the field. Figures 11 and 12 were produced to test the IS-SRMP algorithm when data does not contain near-offset information. Ten null-traces surrounding the source were substituted in the gather shown in Figure 2, which corresponds to a gap of 200 m. There is some dimming near zero angle in the primary events, and a small deviation in the continuity of the curvature of the predicted multiples.

Figure 11 about here

In the interest of direct comparison, the adaptive subtraction parameters were kept constant for both Figures 10 and 12. The faint energy in the center panel of Figure 12 above the second reflector indicates that the same parameters for the adaptive subtraction are not as appropriate for this image volume. However, the remainder of multiple energy is easily removed from the final result when the subtraction is better tuned.

Figure 12 about here

Sigsbee2b

The top panel in Figure 13 shows the bottom third of the multiple contaminated image produced with the Sigsbee2b synthetic data. The bottom image was produced with the data volume without multiples. The center image is the result of predicting the multiples during shot-profile migration of data containing multiples and removing them from the top image. The point diffractors masked in the top image are much better realized in the subtraction result. The multiples in the sedimentary section before $x = 10$ km are almost perfectly removed except for some up-right dipping energy at $x = 7$ km emerging from the basement reflector. Several events between $x = 10 - 19$ km are much more continuous and interpretable.

Figure 13 about here

Gulf of Mexico data

The top panel in Figure 14 shows the bottom half of the multiple contaminated image produced with the Gulf of Mexico data. The center panel is the multiple prediction generated during shot-profile migration. The bottom panel is the subtraction result. The subtraction still contains some residual multiples associated with the salt body. Because these events are well predicted in the center panel, it is possible that the prediction could improve with more diligent adaptive subtraction. Most of the migration diffraction energy associated with the rugose salt surfaces has been attenuated. Many diffracted multiples associated with the 3D nature of the salt body have been removed around $x = 7,20$ km. Primaries at $z = 4.5$ km on the left edge of the image have been brought out and may suggest an anticlynal structure.

Figure 14 about here

DISCUSSION AND CONCLUSIONS

Image space SRMP produces a multiple prediction by convolving the data with itself at every subsurface depth level during the course of a shot-profile migration. The result is the same as migrating the conventional data-space multiple prediction (SRMP). This method is most convenient with shot-profile migration strategies since the convolution operation must operate on distinct gathers rather than the combinations thereof produced by resorting to CMP coordinates. The simplicity of this approach can immediately be leveraged to manufacture the image-space multiple prediction directly from any shot-profile migration program. The method is immediately applicable to 3D, and non-zero subsurface-offset and angle. Any migration algorithm that maintains separate up-coming and down-going wavefields and uses a combinatory imaging condition (e.g. planewave and reverse-time migrations) can be easily modified to produce an IS-SRMP volume.

Importantly, split-spread gathers must be pre-computed via reciprocity for data collected with off-end acquisition geometries. Off-end gathers will not contain (nor therefore predict) emerging rays which pierce the acquisition surface in front of the boat. This may increase the size of the computational domain used for propagating each individual shot-record. The cost increase by performing two imaging conditions is not severe, as the cost of calculating an imaging condition with in-line offsets is usually a fraction of the cost of a shot-profile migration. Therefore, whenever a shot-profile migration is being performed, it may be advantageous to generate the IS-SRMP even if a data-space elimination effort has already been performed, especially when the adaptive subtraction leaves some multiple energy in the final result.

Given a reasonably accurate velocity model for migration, it is only necessary to compute $O(10)$ subsurface offsets. This results in many fewer traces involved in calculating the multiple prediction than the $O(1000)$ offsets collected at the surface. This savings will be reduced however by the need to convolve the traces at every depth level, $O(100)$, of the image-space rather than just at the surface. Whatever the balance of floating-point operations for a particular survey, the convenience of being able to manufacture the multiple prediction during another required processing step will save file manipulation, sorting, and overhead costs. Furthermore, this technique can also be used in a target oriented fashion by simply not calculating the multiple prediction at shallow depths where it is not required.

The quality of the multiple prediction produced in the image-space with this technique is independent of the accuracy of the velocity model used during the migration. The multiple prediction, propagated with the same velocity model, will be kinematically accurate with the location of any multiples in the migrated image. Though both the image and the multiple prediction may be incorrect due to the use of an inaccurate velocity model, it has to correspond with the image constructed with the same extrapolation operators and velocity model. Due to the squaring of the wavelet when

convolving the data, the multiple prediction can not be directly subtracted from the data or the image.

While IS-SRMP, by definition, produces only surface-related multiples, the technique could be manipulated to address strong multiple generators in the subsurface. A layer-stripping type approach derived in parallel to the DSR multiple prediction (Malcolm et al., 2006) could probably be implemented at the cost of extrapolating a third (in addition to the upcoming and downgoing) wavefield.

ACKNOWLEDGMENTS

Reviewers C.P.A Wapenaar, Eric Verschuur, and Paul Sava all made insightful comments to drafts of this manuscript that substantially improved its quality.

REFERENCES

Alvarez, G., B. Biondi, and A. Guitton, 2004, Attenuation of diffracted multiples in angle domain common image gathers: 74th Ann. Internat. Mtg., Soc. of Expl. Geophys., Expanded Abstracts, 1301–1304.

Anstey, N. A. and P. Newman, 1966, The sectional auto-correlogram and the sectional retro-correlogram: Geophys. Prosp., **14**, no. 4, 389–426.

Baysal, E., D. D. Kosloff, and J. W. C. Sherwood, 1983, Reverse time migration: Geophysics, **48**, no. 11, 1514–1524.

Berkhout, A. J. and D. J. Verschuur, 1997, Estimation of multiple scattering by iterative inversion, part I: Theoretical considerations: Geophysics, **62**, no. 05, 1586–1595.

Biersteker, J., 2001, MAGIC: Shell's surface multiple attenuation technique: SEG, 71st Annual International Meeting, 1301–1304.

Claerbout, J. and S. Fomel, 2002, Image Estimation by Example: Geophysical soundings image construction: Class notes, http://sepwww.stanford.edu/sep/prof/index.html.

Claerbout, J. F., 1971, Toward a unified theory of reflector mapping: Geophysics, **36**, no. 03, 467–481.

Guitton, A., 2005, Multiple attenuation in complex geology with a pattern-based approach: Geophysics, **70**, no. 4, V97–V107.

Kessinger, W., 1992, Extended split-step Fourier migration: SEG, 62nd Annual International Meeting, 917–920.

Malcolm, A. E., M. V. de Hoop, and H. Calandra, 2006, Identification of image artifacts due to internal multiples: Submitted to Geophysics.

Rickett, J. E. and P. C. Sava, 2002, Offset and angle-domain common image-point gathers for shot-profile migration: Geophysics, **67**, no. 03, 883–889.

Sava, P. and A. Guitton, 2003, Multiple attenuation in the image space: 73rd Ann. Internat. Mtg., Soc. of Expl. Geophys., Expanded Abstracts, 1933–1936.

Sava, P. and A. Guitton, 2005, Multiple attenuation in the image space: Geophysics, **70**, V10–V20.

Shan, G. and A. Guitton, 2004, Migration of surface-related multiples: tests on the Sigsbee2B dataset: 74th Ann. Internat. Mtg., Soc. of Expl. Geophys., Expanded Abstracts, 1285–1288.

Tsai, C. J., 1985, Use of autoconvolution to suppress first-order long-period multiples: Geophysics, **50**, no. 09, 1410–1425.

Verschuur, D. J., A. J. Berkhout, and C. P. A. Wapenaar, 1992, Adaptive surface-related multiple elimination: Geophysics, **57**, no. 09, 1166–1177.

Weglein, A. B., 1999, Multiple attenuation: An overview of recent advances and the road ahead (1999): The Leading Edge, **18**, no. 1, 40–44.

LIST OF FIGURES

9 Angle-domain image gathers from a flat-layer model. Left to right: Conventional image, multiple prediction, prediction matched to data.

10 Angle-domain image gathers from a flat-layer model. Left to right: Subtraction of matched multiple prediction from data, subtraction matched to data, original data.

11 Angle-domain image gathers from a flat-layer model with missing near offsets. Left to right: Conventional image, multiple prediction, prediction matched to data.

12 Angle-domain image gathers from a flat-layer model with missing near offsets. Left to right: Subtraction of matched multiple prediction from data, subtraction matched to data, original data.

13 Bottom third of the zero-offset image produced with the Sigsbee2B synthetic. Top to bottom: Image with primaries and multiples, subtraction result, image produced from data without multiples.

14 Bottom half of the zero-offset image produced with the Mississippi Canyon, Gulf of Mexico, data provided by Western-Geco. Top to bottom: Image with primaries and multiples, image-space multiple prediction, subtraction result.

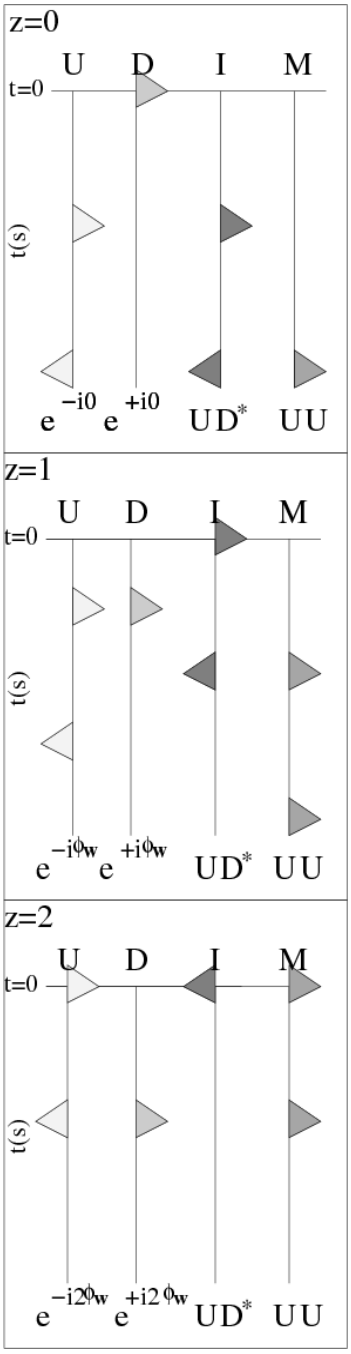

Figure 1.

Brad Artman – GEO-2006-0199-R1

file name: Fig/GEO-2006-0199-R1-fig1.ps dimensions: width=1.8in,height=7in

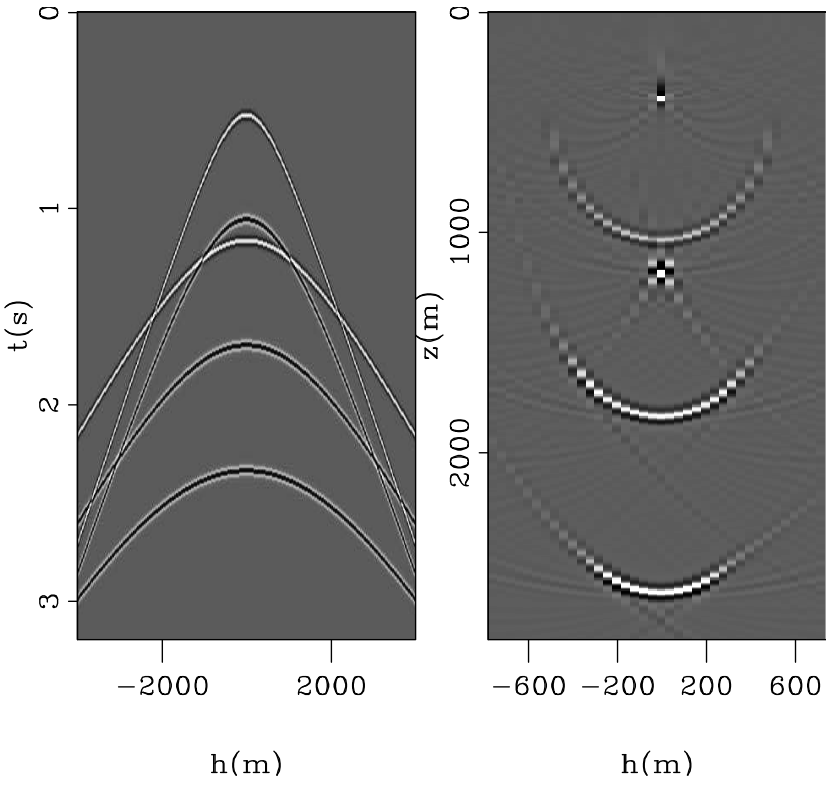

Figure 2.

Brad Artman – GEO-2006-0199-R1

file name: Fig/GEO-2006-0199-R1-fig2.ps dimensions: height=4in

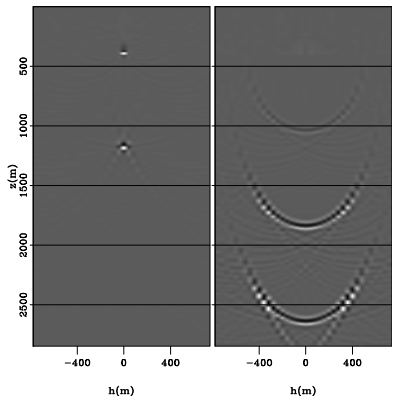

Figure 3.

Brad Artman – GEO-2006-0199-R1

file name: Fig/GEO-2006-0199-R1-fig3.ps dimensions: width=2in

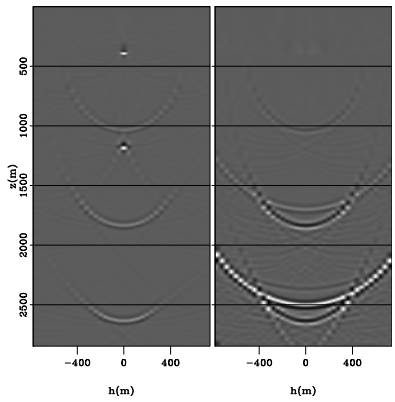

Figure 4.

Brad Artman – GEO-2006-0199-R1

file name: Fig/GEO-2006-0199-R1-fig4.ps dimensions: width=2in

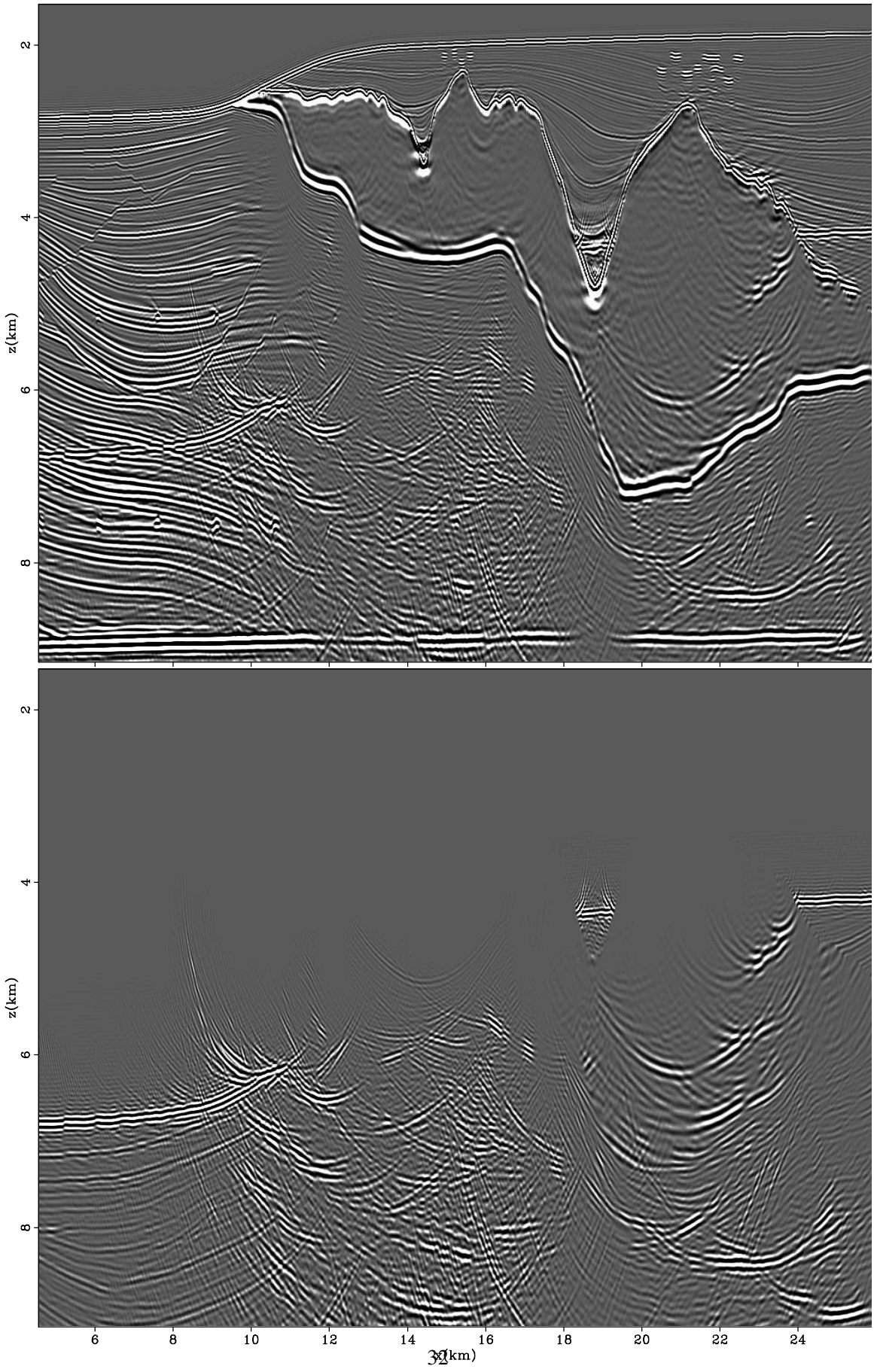

Figure 5

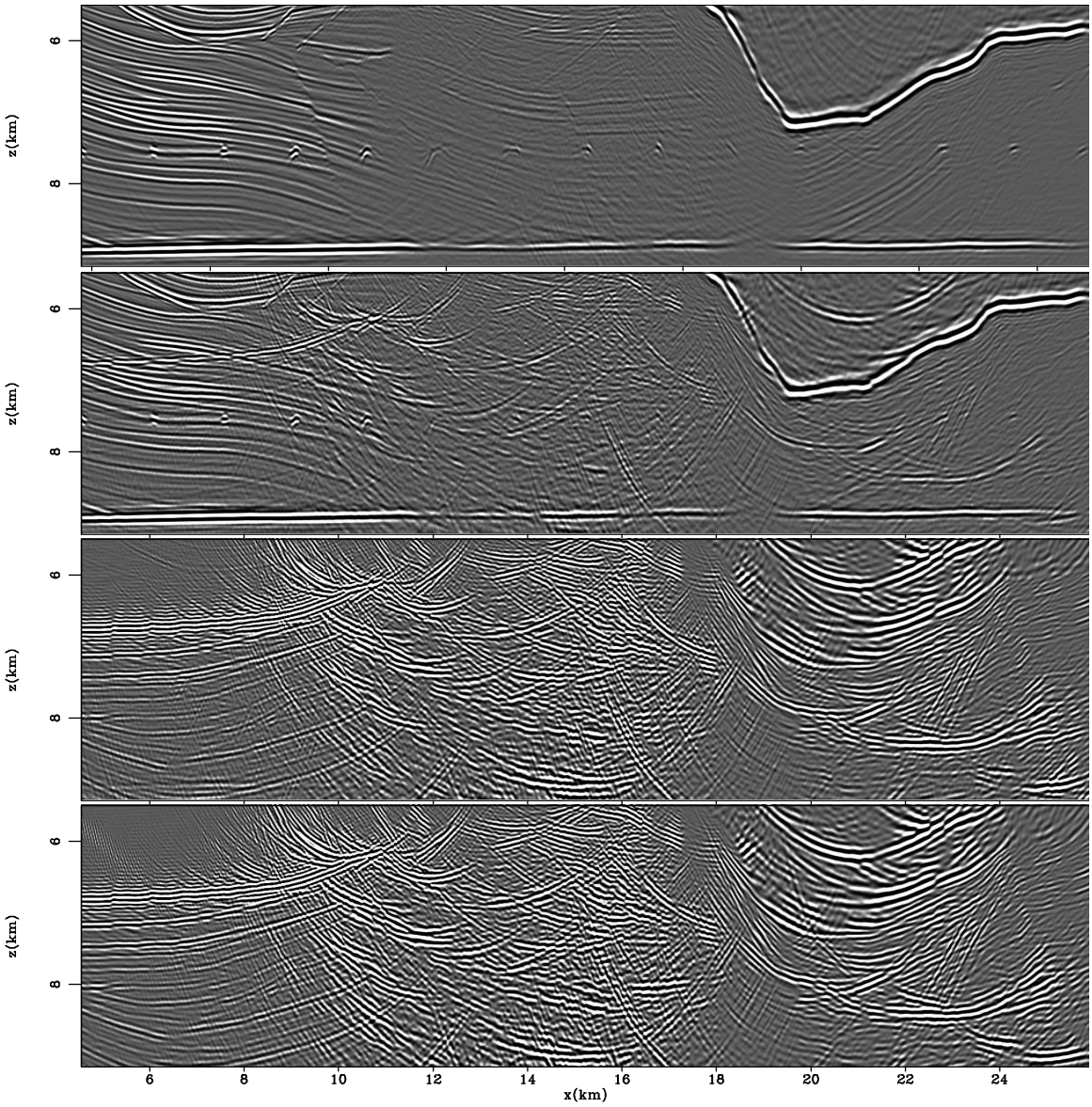

Figure 6.

Brad Artman – GEO-2006-0199-R1

file name: Fig/GEO-2006-0199-R1-fig6.ps dimensions: width=6.0in

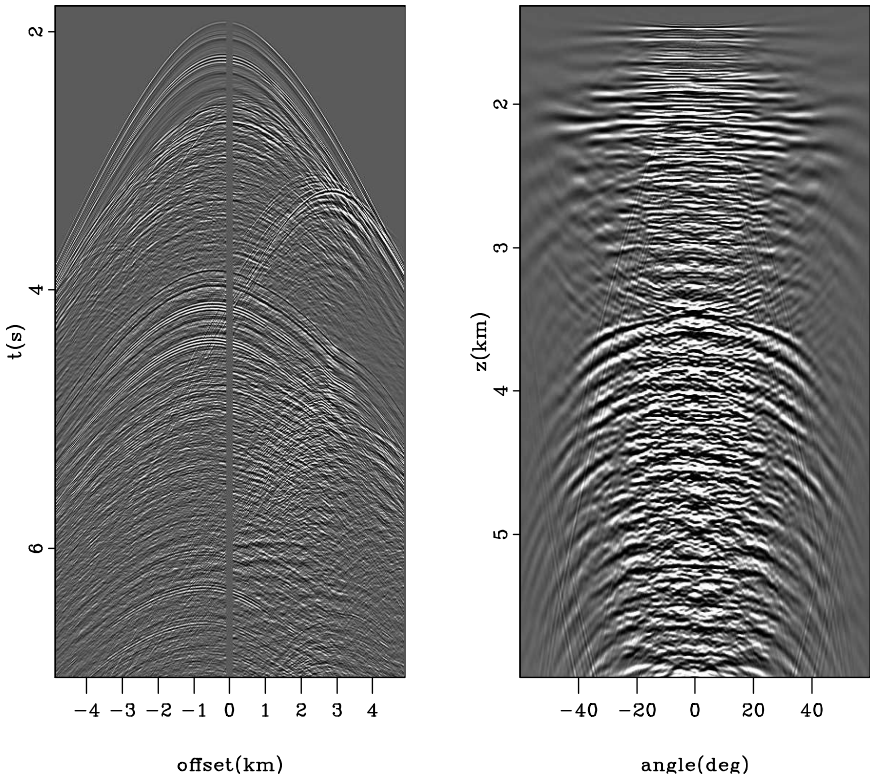

Figure 7.

Brad Artman – GEO-2006-0199-R1

file name: Fig/GEO-2006-0199-R1-fig7.ps dimensions: height=4in

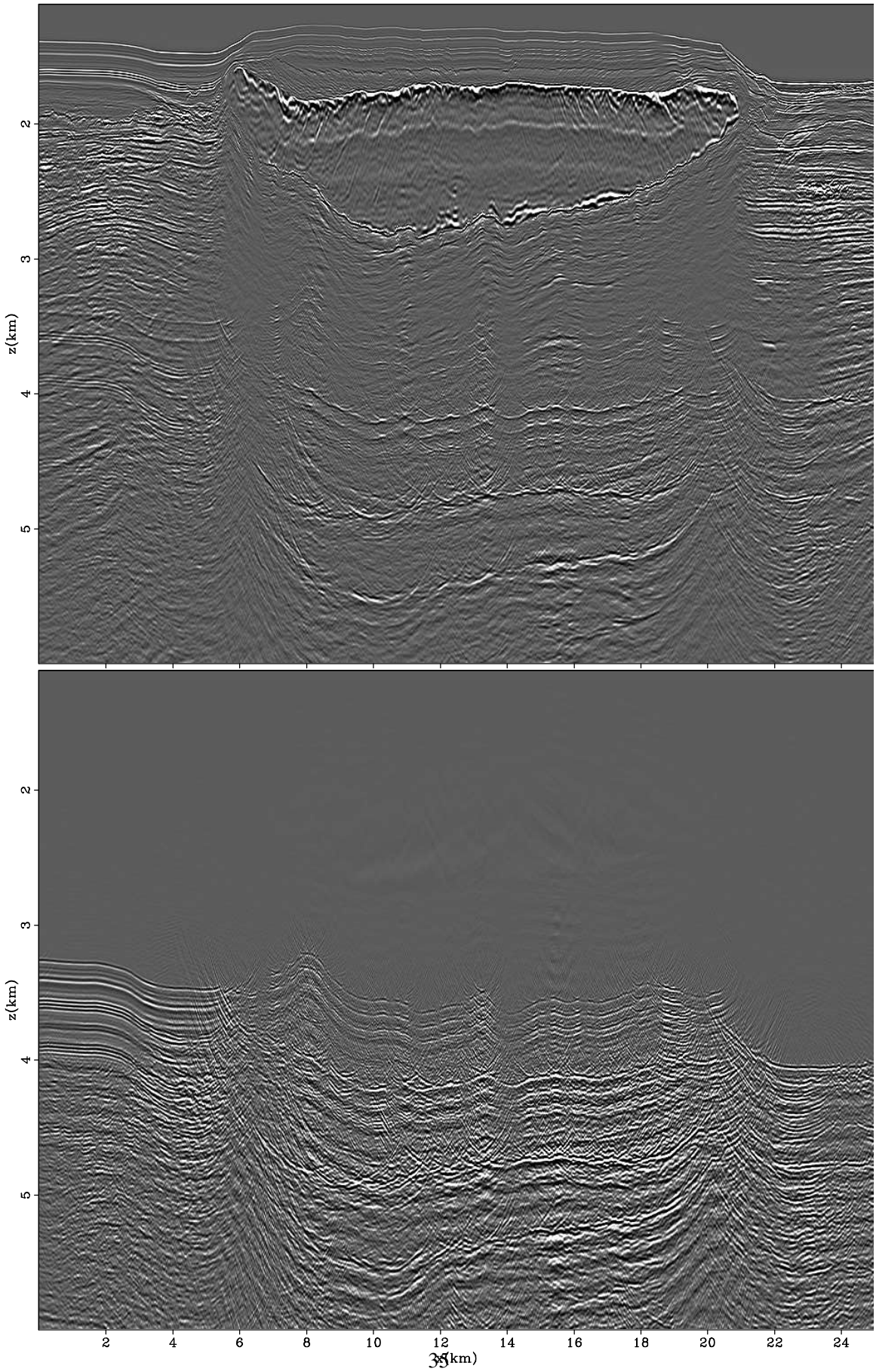

Figure 8

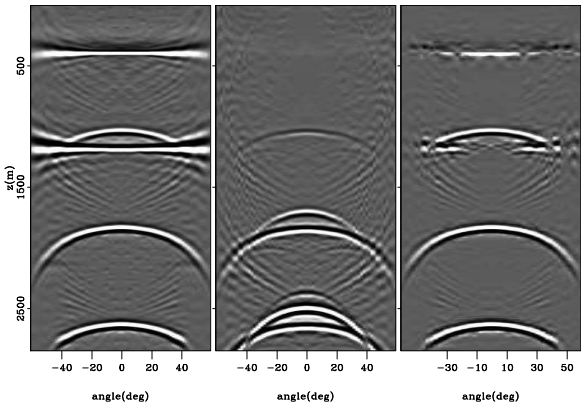

Figure 9.

Brad Artman – GEO-2006-0199-R1

file name: Fig/GEO-2006-0199-R1-fig9.ps dimensions: width=3.0in

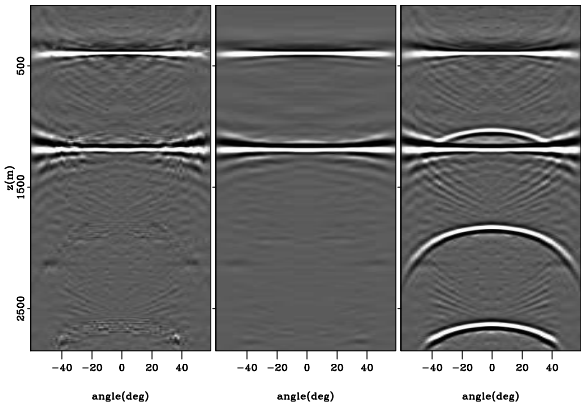

Figure 10.

Brad Artman – GEO-2006-0199-R1

file name: Fig/GEO-2006-0199-R1-fig10.ps dimensions: width=3.0in

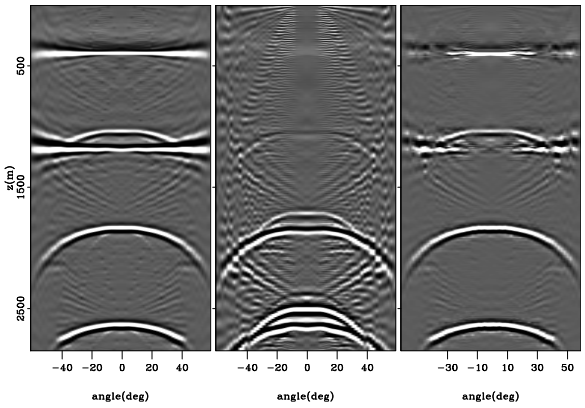

Figure 11.

Brad Artman – GEO-2006-0199-R1

file name: Fig/GEO-2006-0199-R1-fig11.ps dimensions: width=3.0in

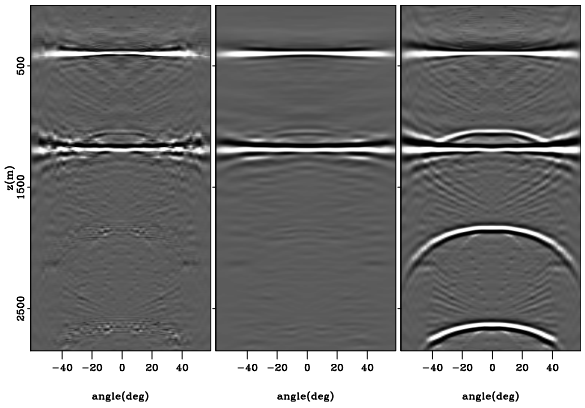

Figure 12.

Brad Artman – GEO-2006-0199-R1

file name: Fig/GEO-2006-0199-R1-fig12.ps dimensions: width=3.0in

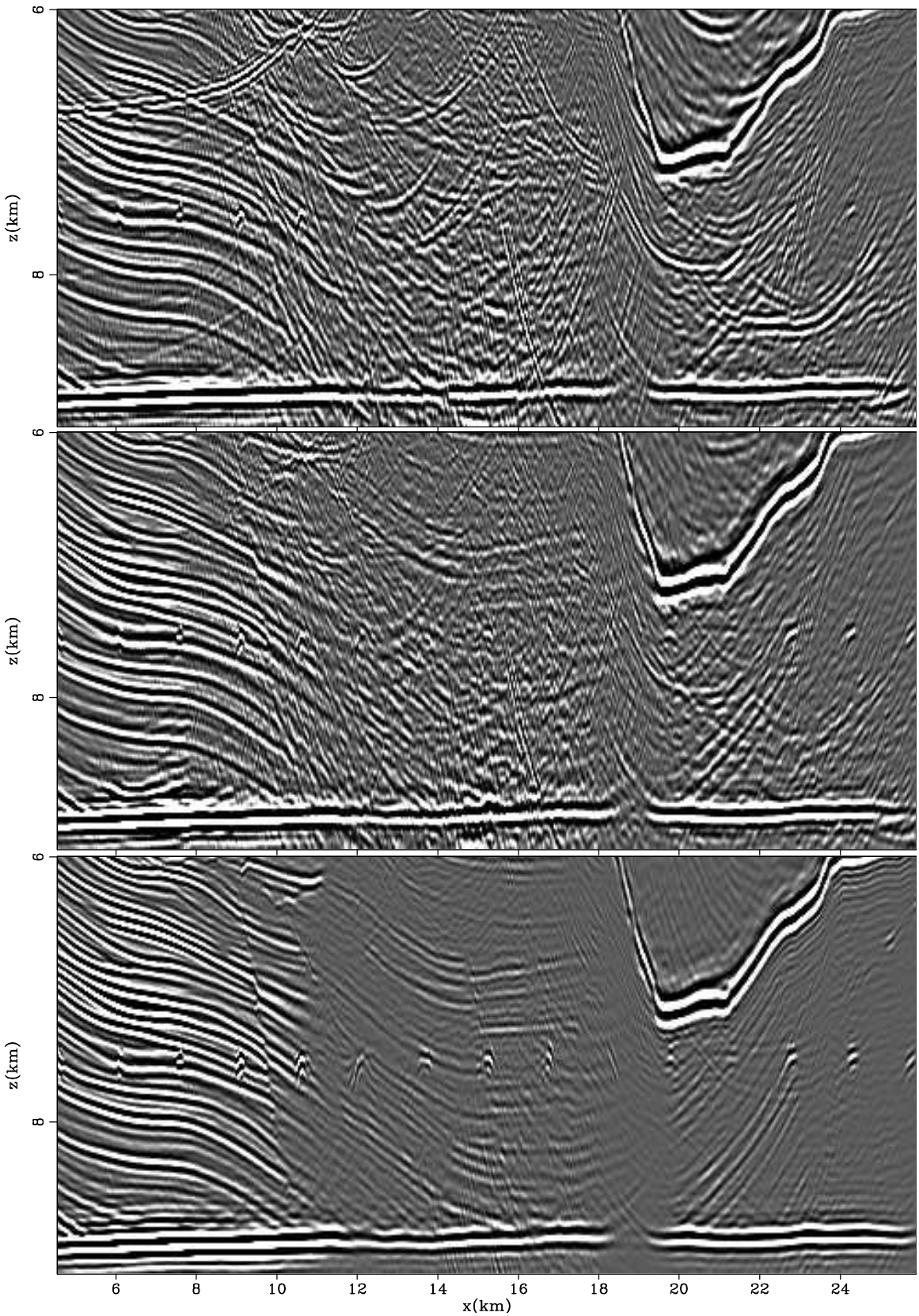

Figure 13.

file name: Fig/GEO-2006-0199-R1-fig13.ps dimensions: width=6in

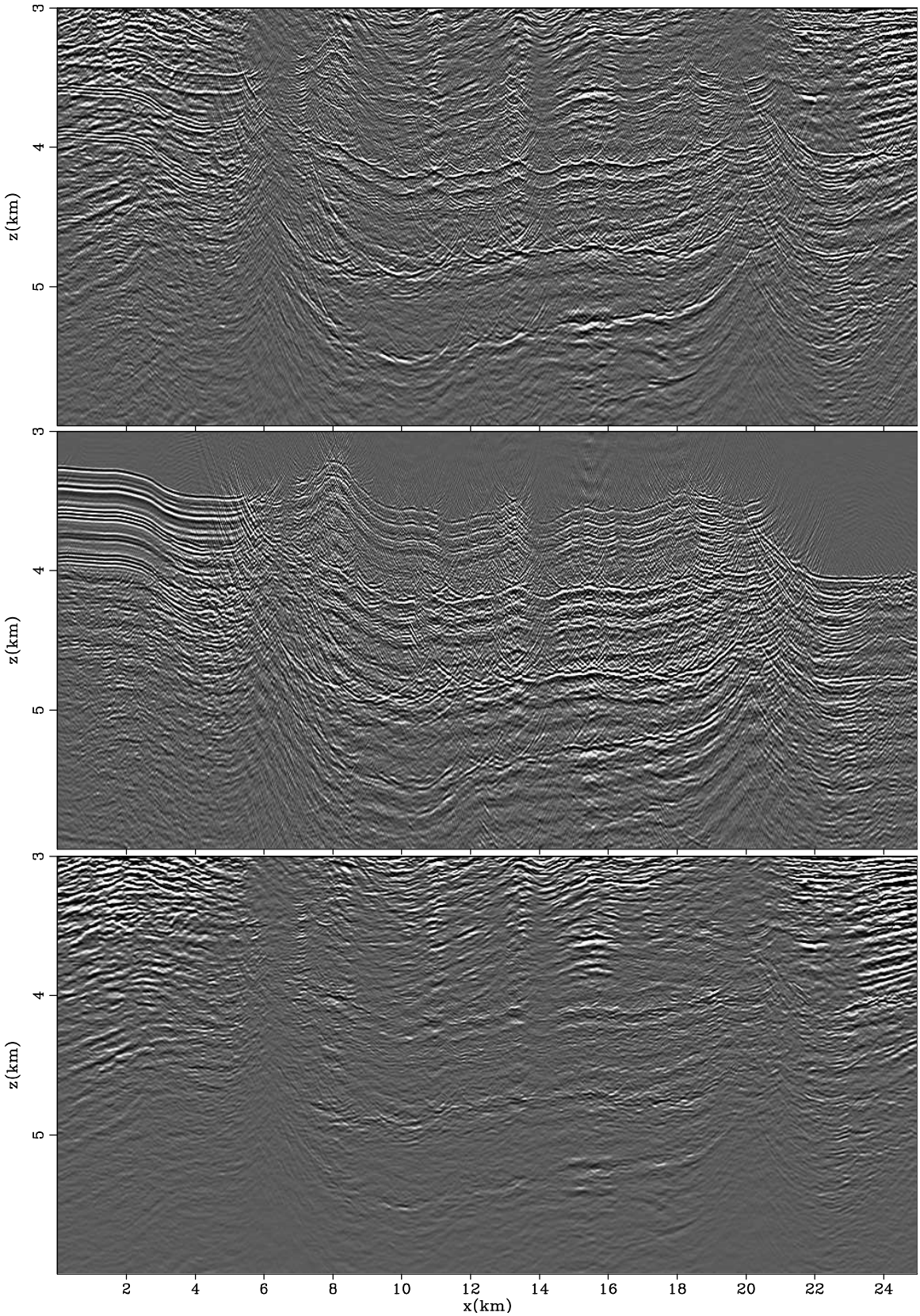

Figure 14.

file name: Fig/GEO-2006-0199-R1-fig14.ps dimensions: width=6in